Fast Volumetric Radiofrequency Current Density Imaging

K. Shultz[1], J. Pauly[1], and G. Scott[1]

[1]Electrical Engineering, Stanford University, Stanford, CA, United States

Introduction: Radiofrequency current density imaging (RFCDI) measures currents at the Larmor frequency [1]. It is potentially useful for applications such as predicting and monitoring RF ablation treatment patterns or measuring the effectiveness of pacemaker insulators. Currents at the Larmor frequency create magnetic fields that act as an effective B_1 field, exciting magnetization. By measuring these fields with Actual Flip-angle Imaging (AFI) [2], a fast B_1 mapping method, volumetric current density can be measured with scan times of only a few minutes. Using the AFI sequence for current density imaging is practical in an ablation environment because the power levels are much lower than the power used for ablation. For example, pulmonary vein ablation uses power levels on the order of 50W for durations of one to two minutes [3], whereas the AFI sequence used here has similar power levels and duration, but only a 1% duty cycle. RFCDI can be used to monitor ablation without incidentally ablating tissue itself.
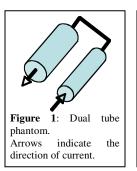

Figure 1: Dual tube phantom. Arrows indicate the direction of current.

Figure 2: Magnitude image of dual tube phantom.

Theory & Methods: With Ampere's Law, current density can be calculated from the local magnetic field. When the current is at the Larmor frequency, its associated field acts as a B_1 field. Previously, RF currents were imaged using an external B_1 excitation in combination with the field from the current [4]. Using a B_1 mapping sequence with the current acting as the only excitation allows for faster acquisition of RF field measurements. The measured magnetic fields can be used to calculate the current density component along the main B_0 field of the magnet. With a volumetric data set, the full current density vector can potentially be reconstructed [5].

AFI [2] is a steady state sequence that allows for faster, higher-SNR B_1 measurements than commonly used techniques such as the double-angle method. The AFI sequence uses two alternating TR lengths to allow differing amounts of T_1 recovery between them. As long as the first TR is short compared to T_1, the ratio of the signals from the two TRs is dependant on the B_1 magnitude but independent of T_1. AFI has a speed advantage over the standard double angle method, which requires long TRs to allow for full magnetization recovery, and an SNR advantage over the saturated double angle method [6], in which magnetization must recover from full saturation.

Figure 3: B_x (left) and B_y (right) maps. Positive fields are tinted red, negative blue. The magnetic fields from each tube circulate in opposite directions, creating stronger fields in the center where the fields reinforce each other.

Experiments were run on a 1.5T GE Signa scanner using an external Medusa console [6] to control the RF and gradient fields. The AFI sequence parameters were TR_1=25ms, TR_1/TR_2 ratio=8, 64x64x32 matrix with 1.4x1.4x3.8mm resolution, for a scan time of one minute. A flyback-EPI readout with 8 echoes was used to accelerate the acquisition. The phantom consisted of two tubes of NaCl solution (see Figures 1 and 2). Both tubes had the same conductivity but different radii. The current flowed down one tube and back the other, creating opposing directions of current. The total current in each tube was the same, but due to their different diameters, the current densities were different. The RF excitation was created by transmitting a 1.5ms hard pulse of Larmor frequency current through the phantom, with a quadrature head coil used to receive. Two data sets were acquired, roughly halving the magnitude of the current for the second acquisition, to cover the full range of B_1 magnitudes created by the current. Phase variations due to imperfect gradient shimming were measured by using the head coil to transmit and were then removed. The phase of the B_1 map was used to separate B_x and B_y. A Sobel derivative was used to calculate the current density from the magnetic fields.

Figure 4: Current density in series configuration. The top tube has negatively directed current, while the bottom tube has positively directed current. The magnitude of the current density is larger in the smaller bottom tube.

Results: The B_1 maps for the central plane (Figure 3) show the expected fields. There are strong x-directed fields between the tubes, where the oppositely directed currents create reinforcing fields. There are weaker fields in the periphery, where the fields are opposed and cancel each other, including a contour of zero magnetic field where the fields from the two tubes cancel completely. Figure 4 shows opposite directions of current in each tube. The current image is noisier because it is created from spatial derivatives of the B_1 images. The bottom tube has a greater density of current due to its smaller cross section. There are edge effects at the tube boundaries due to the derivative operator acting on a signal void.
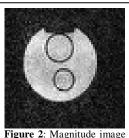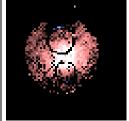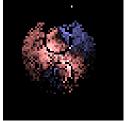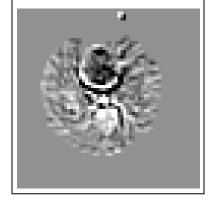
Discussion & Conclusions: Using the AFI sequence to measure B_1 fields generated by an RF current allows a full volumetric measurement of one component of the RF current density in a total scan time of two minutes. Significant work needs to be done to improve SNR. This can be accomplished by optimizing the AFI sequence, increasing the voxel size, and using a surface coil rather than the head coil. Additionally, weighting the extremes of k-space more heavily in acquisition will improve SNR, because the spatial derivatives used to calculate the current density are equivalent to linear weightings in k-space. Future experimental work will involve testing the technique in heterogeneous media and reconstructing the missing current components to achieve full-vector current density measurements. Fast, full-vector RFCDI has many potential applications such as prediction of heat deposition in RF ablation, monitoring of conductivity changes during ablation, and safety monitoring of induced and leakage current.

References: [1]G. Scott et al, Magn. Reson. Med. 28:186, 1992. [2]V. Yarnykh, Magn. Reson. Med. 57:192, 2007. [3]Guy, D.J.R. et al, Pacing and Clinical Electrophysiology, 26: 1379, 2003. [4]G. Scott et al, Magn. Reson. Med. 33:355, 1995. [5]K. Shultz et al, Proc. 15th ISMRM, p1131, 2007. [6]C. Cunningham et al, Magn. Reson. Med. 55:326, 2006. [7]P. Stang et al, Proc. 15th ISMRM, p925, 2007.